Investigation on Gaseous Fuels Interchangeability with an Extended Zero-dimensional Engine Model

La Xiang[a, b], Gerasimos Theotokatos[b], Yu Ding[a,*]

[a] *College of Power and Energy Engineering, Harbin Engineering University, Harbin 150001, China*

[b] *Maritime Safety Research Centre, Department of Naval Architecture, Ocean and Marine Engineering, University of Strathclyde, Glasgow, Scotland, UK*

[*] *Corresponding author: e-mail: dingyu@hrbeu.edu.cn; address: No. 145, Nantong Street, 150001, Harbin, China*

0. Abstract

As the gaseous fuels interchangeability, which requires that the two gaseous fuels must be nearly identical in terms of their combustion characteristics and result in a similar engine performance, is important for internal combustion engines operation in cases of the fuel composition variation or the main fuel supply failure. In such cases, simulation tools of sufficient accuracy can be effectively employed in fuel interchangeability studies as well as for predicting the engine performance and emissions. In this study, a zero-dimensional diesel engine model is extended for simulating multi-fuel engines by considering the thermodynamic properties of the employed fuels. The model is verified against experimental data and subsequently employed to investigate the performance and knocking resistance of an SI engine operating with interchanged gaseous fuels mixtures. The derived results demonstrate that the Wobbe Index estimation is not sufficient for the characterisation of the engine performance and therefore simulation must be used for the accurate engine performance prediction with fuels interchangeability. The addition of either carbon dioxide or nitrogen results in reducing the knocking probability and retarding the knocking onset crank angle. It is inferred that the carbon dioxide addition is more effective than the nitrogen addition and concluded that the proposed model for multi-fuel engines provides results of [illegible] rformance and knocking resistance.

Keywords: fuel interchangeability, thermodynamic properties, Wobbe Index, engine performance, knocking resistance

1. Introduction

Gas engines have been increasingly employed as prime movers in transport vehicles [1] and electricity generators [2]. Natural gas (NG) is typically used as the primary fuel for gas engines [3], whilst biogas and pyrolysis gas are also used in countries with abundant biomass or energetic waste resources [4]. Gaseous fuels are usually non-homogeneous mixtures with their composition being highly dependent on the production field (natural gas) or the production process (biomass produced fuels) [5]. In some regions, the pipeline natural gas is mixed with other gaseous fuels or inert gases in order to maintain specific fuel properties [4], which makes the fuel composition greatly varying. The interchangeability between gaseous fuels becomes necessary for gas engines when the fuel composition varies or the main gaseous fuel supply fails. As the fuel composition plays a key role in determining the fuel thermodynamic properties (heating value, specific energy, specific heat, etc.), the fuel composition variation significantly affects the engine performance [6] and emissions [5]. In this respect, the investigation of the fuel interchangeability between gaseous fuels in combustion engines is a topic of great importance.

The fuel interchangeability requires that the two gaseous fuels must be nearly identical in terms of their combustion characteristics, efficiency and flame properties. Three main methods have been proposed for estimating the interchangeability of gaseous fuels; in specific, the Weaver method, the American Gas Association (AGA) method and the Wobbe Index (WI). The WI is widely-used in engine applications to assess the interchangeability of gaseous fuels, as the flame indices defined in the Weaver method [7] and the AGA method [8] are more suitable for domestic burners rather than internal combustion engines [9]. Klimstra [10] introduced the WI as a criterion for gaseous fuels interchangeability and concluded that the fuel composition variations appear not to induce noticeable changes to the air-fuel ratio and the combustion velocity when the WI remains constant, whilst the explosion limits and the knock resistance varied to a moderate extent with the fuel composition variations. Karavalakis et al. [11] measured the exhaust emissions of a Cummins 8.3 L natural gas engine operating on seven different fuel gas blends with varying WI and Methane Number (MN). The higher hydrocarbons gaseous fuels were proved to yield higher carbon dioxide (CO_2) and nitrogen oxide (NO_x) emissions, whilst the total hydrocarbons (THC), methane (CH_4), carbon monoxide (CO) and particulate matter (PM) emissions reduced for the fuels with higher hydrocarbons and higher WI. Cardona [12] presented an analysis of the interchangeability between a biogas/propane/hydrogen mixture (50% biogas / 40% propane / 10% hydrogen in volume) and methane in a contoured slot burner, which is based on the WI and the laminar burning velocity, concluding that the variations of these properties between the tested fuels did not exceed 10% of the methane properties; thus enabling the tested mixture to substitute the natural gas. By employing graphical interchangeability methods based on the WI and the combustion potential [13] as well as several multi-index methods [14], it was demonstrated that the plastic pyrolysis gas is a suitable alternative to the natural gas. The previously discussed experimental studies [10-14] combined the WI with other specific indices for accurately evaluating the gaseous fuel interchangeability. However, experimental studies require considerable resources and are costly, therefore they are not handy for a quick and reliable evaluation of the fuels interchangeability.

In this respect, a more cost effective method for investigating the fuel interchangeability is by using simulation tools. Engine modelling and simulation enable to obtain a better understanding of the engine components processes characteristics comprehensively during the engine design phase; therefore they can be employed for evaluating the gaseous fuel interchangeability. In general, simulation models for internal combustion engines can be classified as follows (from simpler to more complicated): mean value models, zero-dimensional or one-dimensional models, and multi-dimensional models [15]. The mean value models are usually set up and calibrated by using a large amount of engine test data and are not capable of predicting the in-cylinder parameters variations [16]. The multi-dimensional simulation models (or Computational Fluid Dynamics model) provide the most detailed representation of the in-modelled engine components, and therefore they are appropriate for engine components design studies as well as for obtaining better insight of the involved thermo-physical processes [17]. The zero-dimensional models employ the assumption of uniform variations of the working medium state and concentration within the engine components and is a quite an effective predictive model approach, which is extensively used for engine performance/emissions prediction [18]. For modelling the engine cylinders combustion process, a number of approaches can be used from single zone [19] to multi−zone phenomenological models [20].

For the natural gas engines modelling, one of the key objectives is to predict the knocking phenomenon which constrains the further engine thermal efficiency improvement [21]. In this respect, a two-zone zero-dimensional model could be an effective tool for both the engine performance and knocking prediction, as it is capable of characterizing the end-gas temperature with the simplest combustion zone division [22] and it is a compromise between the required model complexity, input data and computational time.

Notwithstanding the above, independently of the engine model type is used for the fuel interchangeability investigation, the thermodynamic parameters of the fuel and the in-cylinder gas (heating value, internal energy, enthalpy, specific heat, etc.) must be determined by employing a suitable method. The most frequently employed method is to assume the thermodynamic parameters as constant according to empirical [23] or experimental data [24], or calculate them by the properties and mass fraction assuming that the working medium consists of several basic species [16] . It is reported in [26] that the latter method can achieve higher accuracy as it considers the variation of in-cylinder working medium composition and thermodynamic properties [26]. Ding [27] investigated the thermodynamic properties of the fuel and the in-cylinder working medium in diesel engines by using a first principles calculation method considering the thermodynamic properties functions of the working medium temperature and composition. Neto [28] used the Density Functional Theory (DFT) and the canonical ensemble to investigate the thermodynamic properties of the major molecules compounds at the gaseous phase of fuels like gasoline, ethanol, and gasoline-ethanol mixture, including the internal energy, enthalpy, entropy and Gibbs free energy. Li [29] analysed the average thermodynamic properties of the NG–air mixture, such as the specific heat ratio and the specific heat capacity as functions of the total equivalence ratio by using thermodynamic relations and the ideal gas equation. These studies focused on the in-cylinder thermodynamic parameters of specific liquid or gaseous fuels and cannot be used directly for the interchangeability investigation of gaseous fuels, which requires approaches with great flexibility in the fuel types and compositions.

From the proceeding analysis it is deduced that most of the published gaseous fuel interchangeability studies were carried out by employing experimental methods, which are case dependent, time-consuming and involve considerable cost. On the other hand, a two-zone zero-dimensional model can be an effective tool to investigate the fuel interchangeability as well as the knocking performance of internal combustion engines. In addition, most of the numerical methods for thermodynamic properties estimation are limited to specific fuel types, which are not applicable for the model development of an internal combustion engine running on flexible fuels.

In this respect, this study aims at extending a zero-dimensional model, which was initially developed for diesel engines, taking into consideration the thermodynamic properties of a number gaseous fuels −in specific natural gas (NG) and hydrogen (H_2)− as well as their combustion products, thus allowing for the development of a model capable of the performance prediction of multi-fuel engines. The model applicability is verified by using experimental data from single-fuel and multi-fuel engines, including a diesel engine, a natural gas spark-ignited (SI) engine, a dual-fuel engine and a tri-fuel engine. Subsequently, the validated model is used to investigate the interchangeability between gaseous fuels with same WI and the influence of inert gases (carbon dioxide and nitrogen) addition on the engine knocking resistance.

The novelty of this study is summarised as follows: (a) Extension of a zero-dimensional single-zone model initially developed for diesel engines to a two-zone zero-dimensional model, which is capable of predicting the performance of single-fuel engines and multi-fuel engines; (b) investigation of the engine performance with fuels with the same WI; and (c) Investigation of the influence of the inert gases addition on the engine knocking performance during the fuel interchangeability by employing the developed two-zone knocking model.

2. Model Description

This section described the two-zone zero-dimensional model employed in this study in order to investigate the gaseous fuel interchangeability. A number of submodels are used for estimating the combustion heat release rate, the heat transfer from the gas to the engine cylinder walls, the working medium properties, as well as the knocking prediction. The developed model was implemented in the MATLAB/SIMULINK computational environment.

2.1 Calculation Principles

The proposed model simulates the closed cycle of one engine cylinder, i.e., the compression, combustion and expansion stage. The specific assumptions for developing the model are outlined as follows.

1) The working medium inside the cylinder is uniformly distributed, which indicates that its pressure, temperature and concentration are the same throughout the cylinder.
2) The in-cylinder gas is considered to be ideal but non-perfect. Thus, its thermodynamic properties can be calculated as functions of its temperature and composition.
3) Dissociation effects are not taken into account. Only the hydrocarbons (HC), sulphur (S) and oxygen (O_2) take part in the reaction and end up with complete combustion products like nitrogen (N_2), oxygen (O_2), argon (Ar), carbon dioxide (CO_2) and water (H_2O).

4) Blowby and valves leakage in the engine cylinder are not considered.

2.1.1 Heat Release

Semi-empirical formulas are usually employed to simulate the combustion Heat Release Rate (HRR). Typically, the HRR determining methods include the Triangular Exothermic function, the Polygon-hyperbola function and the Vibe function [30], among which the Vibe function is most widely used. The burnt fuel fraction simulated by a single Vibe function [31] is represented by the following equation:

$$x_b = 1 - e^{-a \cdot \tau_v^{m_v+1}} \tag{1}$$

where, x_b is the burnt fuel fraction; a is the coefficient related to the combustion efficiency, which is usually set at 6.9078 to maintain a combustion efficiency of 99.9%; τ_v is the normalized combustion time; and m_v is the shape factor.

The total heat release in a multi-fuel engine can be obtained by employing several Vibe functions. Generally, two Vibe functions can sufficiently represent the combustion process of a directly injected diesel fuel, which consists of a premixed combustion stage and a diffusion combustion stage. One Vibe function is able to characterize the combustion process of a premixed gas engine as it represents the main characteristics of a premixed combustion. In this study, two parameters, in specific the Total Energy Input (*TEI*) and Accumulated Heat Release (*AHR*) are defined to describe the total heat release calculated by using the lower heating value (LHV) and the combustion heat, by employing Eq (2) and Eq (3), respectively. The *Combustion Heat* (u_{comb}) is the specific heat release corresponding to the specific internal energy difference between the combustion reactants and products [27], which will be described in detail in the following section.

$$TEI = \sum_{i=1}^{N} m_i \cdot LHV \tag{2}$$

$$AHR = \sum_{i=1}^{\mathrm{M}} \int_{SOC_i}^{EOC_i} m_i \cdot \left[b_{i,1} \cdot \dot{x}_{b,i,1} + b_{i,2} \cdot \dot{x}_{b,i,2} \right] \cdot u_{comb,eff,i}\, dt + \sum_{j=1}^{N\text{-}\mathrm{M}} \int_{SOC_j}^{EOC_j} m_j \cdot \dot{x}_{b,j} \cdot u_{comb,j}\, dt \tag{3}$$

where, M is the number of the direct injection liquid fuels; N is the number of all the employed fuels; *SOC* and *EOC* denote the start and end timing of the fuel combustion. *SOC* and *EOC* (for each fuel and Vibe function employed) are estimated by the HRR analysis, which can be either calculated by using the experimentally measured in-cylinder pressure or by using CFD combustion modelling. For per liquid fuel, which requires two Vibe functions to characterise the premixed and diffusion combustion respectively, the *SOCs* and *EOCs* are considered the same for both functions in order to simplify the modelling; m is the injected fuel mass of each fuel; $b_{i,1}$ and $b_{i,2}$ are the weigh factors for premixed combustion stage and diffusion combustion stage of direct injection liquid fuels, $b_{i,1}+ b_{i,2}=1$; m_v is the shape factor; $u_{comb,eff,i}$ is the effective combustion heat of each liquid fuel; $u_{comb,j}$ is the combustion heat of each gaseous fuel.

2.1.2 Heat Transfer

The cylinder walls include three parts: the surface of the cylinder head and valves, the surface of the cylinder liner and the top surface of the piston. The temperature of each part of the heat transfer surface is considered to be constant as its variation is small enough to be neglected compared to the in-cylinder gas temperature. The Woschni model [32] is considered for calculating the instantaneous heat transfer coefficient $\alpha_{g\rightarrow w}$ from the in-cylinder gas to walls. The heat transfer between the working medium and the cylinder walls is calculated according to the following equation:

$$Q_{\text{loss}} = \sum_{1}^{3}\left[\alpha_{g\rightarrow w} \cdot (T - T_{wall,i}) \cdot A_{wall,i}\right] \tag{4}$$

where, $\alpha_{g\rightarrow w}$ is the instantaneous heat transfer coefficient from the in-cylinder gas to the walls; $T_{wall,i}$ is the average wall temperature of each surface. i=1, 2, 3, which represents the cylinder head and valves, the cylinder liner and the cylinder piston respectively; and $A_{wall,i}$ is the heat transfer surface area.

2.1.3 Mass Balance and Composition

In order to estimate the in-cylinder working medium properties in internal combustion engines, the in-cylinder gas is considered as a mixture of several well-defined basic mixtures; in specific, air, gaseous fuel (if any) and stoichiometric gas, whilst all the basic species are considered as ideal but non-perfect. The stoichiometric gas is defined as the complete combustion product of the stoichiometric air-fuel mixture. The constituents of air, gaseous fuel and stoichiometric gas are listed as follows.

1) Air: Fixed-fraction dry air (N_2, O_2, Ar, CO_2) and water vapour (H_2O);
2) Gaseous fuel: methane (CH_4), ethane (C_2H_6), propane (C_3H_8), *n*-butane (*n*-C_4H_{10}), *i*-butane (*i*-C_4H_{10}), pentane (C_5H_{12}), N_2, CO_2 (taking natural gas for example);
3) Stoichiometric gas: N_2, O_2, Ar, CO_2, H_2O.

For direct injection engines, only the air and the stoichiometric gas need to be considered on the assumption that the injected fuel burns immediately after its injection within the engine cylinder. The mass fractions of the different species in the gaseous fuel and the air can be obtained from the fuel type and the ambient air humidity respectively, whilst that of the stoichiometric gas needs to be calculated according to the complete combustion chemical reaction. Assuming that only Hydrocarbons, Sulphur and Oxygen take part in the combustion reaction, the following equation is used for representing the combustion.

$$C_nH_mS_l + \left(n + \frac{m}{4} + l\right)O_2 \longrightarrow nCO_2 + \frac{m}{2}H_2O + lSO_2 \tag{5}$$

For direct injection engines, the instantaneous mass fraction of the in-cylinder air can be calculated by using Eq (6). The two terms of the numerator of the right-hand side represent the initial air mass and accumulated burnt air.

$$x = \frac{m_0 \cdot x_0 - \sigma \cdot \int_{SOC}^{EOC} \xi \cdot dt}{m_0} \tag{6}$$

where, m_0 is the mass of the in-cylinder mixture at Inlet Valves Close (IVC); x_0 is the initial mass fraction of fresh air at IVC; σ is stoichiometric air-fuel ratio; ξ is the combustion rate obtained by Vibe function. For premixed combustion engines, the instantaneous mass fraction of air-fuel mixture can be obtained on the assumption that air and gaseous fuel react at the stoichiometric ratio, according to Eq(7).

$$x = \frac{m_0 \cdot x_1 - (1+\sigma) \cdot \int_{SOC}^{EOC} \xi \cdot dt}{m_0} \tag{7}$$

where, x_1 is the initial mass fraction of air-fuel mixture at IVC.

2.1.4 In-cylinder gas properties

Assuming that the in-cylinder gas behaves as an ideal but non-prefect gas, the thermodynamic parameters of each species only depend on the in-cylinder temperature and can be obtained by the power series equation that varies with the normalized temperature according to Eq (8). Yaws [33] and Borman [34] obtained the fitting coefficients of various types of gases by using experimental methods.

$$c_{p,j} = \sum_{k=1}^{l} a_{k,j}\, \theta^{k-1} \tag{8}$$

where, a_k is the fitting coefficient of specific heat at constant pressure; θ is normalized temperature, $\theta = (T - T_{shift}) / T_{norm}$; T_{shift} is the shift temperature, T_{shift}=0 K; T_{norm} is the normalised reference temperature, T_{norm}=1000 K.

The specific heat at constant volume of each species can be calculated by using the gas constant and the molar mass, according to the following equation.

$$c_{v,j} = c_{p,j} - R_j / M_j \tag{9}$$

The specific enthalpy and internal energy of each species can be calculated by Eq (10) and Eq (11), respectively.

$$h_j = \int c_p dT + h_j^{ref} = \sum_{k=1}^{l} \frac{a_{k,j}}{k} \cdot T_{norm} \cdot \theta^k - \sum_{k=1}^{l} \frac{a_{k,j}}{k} \cdot T_{norm} \cdot \theta_{ref}^k + h_j^{ref} \tag{10}$$

$$u_j = \int c_v dT + u_j^{ref} = h_j - R_j \cdot T \tag{11}$$

where, h_j^{ref} and u_j^{ref} are specific enthalpy and internal energy at standard conditions; θ_{ref} is normalized reference temperature.

Since each species in air, gaseous fuel and stoichiometric gas are considered ideal but non-prefect gases, the mixtures behave as ideal but non-prefect as well. Thus, the specific heat, enthalpy and internal energy of the considered mixtures are functions of the average temperature and their composition. A power series of the normalized temperature is used to fit these property data for all the species and the properties of the mixtures can be obtained considering ideal mixtures.

The in-cylinder working gas properties, i.e. the specific heat, specific enthalpy and specific internal energy, can be calculated by species property data and composition fractions according to the following equation:

$$f(x,T) = \sum_{l}^{L} x_l \left(\sum_{j=1}^{J} x_j \; f_j(T) \right) \tag{12}$$

where, T is the average in-cylinder temperature; $f_j(T)$ is the property data (c_v, h and u) for each basic species; x_j is the mass fraction of the considered mixture constituents; x_l is the mass fraction of air, gaseous fuel and stoichiometric gas.

2.1.5 Combustion Heat

The *Combustion Heat* (u_{comb}) is introduced for calculating the specific heat release by using the difference of the specific internal energy between the combustion reactants and products [27]. Compared to the traditional heating value (HV) determination methods, it considers the influence of instantaneous temperature on the specific heat release. The combustion heat can be calculated by considering the specific internal energy of the fuel, the air and the stoichiometric gas according to the following equation:

$$u_{comb} = u_f + \sigma \cdot u_a - \left(1+\sigma\right) \cdot u_{sg} \tag{13}$$

where, u_f, u_a and u_{sg} are the specific internal energy of the fuel, the air and the stoichiometric gas calculated by using the average cylinder temperature and the gas composition.

For direct injection engines (including liquid and gaseous fuel engines), the energy change caused by the difference between the injection pressure and the in-cylinder pressure must be taken into consideration. In addition, the evaporation heat must also be included in the energy change for the direct injection engines running on liquid fuels. A direct injection diesel engine is taken as an example to illustrate these two parts of the energy change. The energy change during the process of the diesel fuel injection includes two parts: (a) the kinetic energy increase caused by the velocity variation, and (b) the liquid diesel fuel evaporation. E_f is introduced to represent the sum of these two parts of the energy and it can be calculated by the difference between the specific enthalpy of the liquid diesel and the specific internal energy of the evaporated gaseous diesel [27], according to the following equation:

$$\dot{E}_f = \dot{m}_{f,in} \cdot e_f = \dot{m}_{f,in} \cdot \left(h_{f,liquid}^{in+} - u_{f,gas}\right) \tag{14}$$

where, $h_{f,liquid}^{in+}$ is the specific enthalpy of the liquid diesel fuel; $u_{f,gas}$ is the specific internal energy of the evaporated gaseous diesel fuel; $\dot{m}_{f,in}$ is the injected diesel fuel flow rate. Since the injection rate, evaporation rate and combustion rate are assumed to be the same for the zero-dimensional engine modelling, $\dot{m}_{f,in}$ equals the diesel combustion rate ξ_D.

Combining Eq (13), Eq (14) and after some manipulation, Eq (15) is derived, which provides the *Effective Combustion Heat* ($u_{comb,eff}$) for a direct injection engine running on liquid diesel fuel.

$$\begin{aligned} u_{comb,eff,D} &= u_{comb,D} + e_f \\ &= \left[u_{f,D} + \sigma_D \cdot u_a - \left(1+\sigma_D\right) \cdot u_{sg,D}\right] + e_f \end{aligned} \tag{15}$$

where, $u_{comb,D}$ is the combustion heat of diesel fuel calculated by Eq (13); e_f is the specific energy accounting for the injection pressure difference and the fuel evaporation process.

2.1.6 Knocking Prediction

The knocking phenomenon, including conventional knocking and super knocking, is the main obstacle to employ a high compression ratio for improving the thermal efficiency of gas engines. It is generally accepted that the super knocking originates from the pre-ignition in highly boosted gas engines, especially for fuel direct injection engines in the low-speed high-load operating conditions [35]. According to [36], the conventional knocking is associated with auto-ignition in the unburnt zone after the combustion start. As the investigated 2135 NG engine is naturally aspirated, only the conventional knocking phenomenon will be considered in this study. The probability and corresponding crank angle position of knocking can be determined by Eq (16). According to Livengood and Wu [37], knocking occurs when the integral of Eq (16) reaches unity.

$$I = \int_{t=0}^{t_i} \frac{\mathrm{d}t}{\tau} = 1 \tag{16}$$

where τ *(in ms)* is the induction time calculated according to Eq (17) as function of the instantaneous temperature and pressure in unburnt zone; t is the elapsed time from the start of the compression process of the unburnt zone, and t_i is the time of auto-ignition.

$$\tau = 17.68\left(\frac{\mathrm{ON}}{100}\right)^{3.402} p^{-1.7} \exp\left(\frac{3800}{T_2}\right) \tag{17}$$

where ON is the octane number of the fuel; p is absolute pressure in atmosphere, and T_2 is the temperature in unburnt zone.

When the temperature and pressure time variation of the unburnt gas during an individual cycle are known, Eq (16) and Eq (17) can be used to determine whether auto-ignition occurs before the normally propagating flame consumes the unburnt gas.

2.2 Model Calculation Flowchart

Figure 1 shows the calculation flowchart of the prediction model for evaluating the gaseous fuels interchangeability. A zero-dimensional model initially developed for diesel engines is extended with the consideration of the thermodynamic properties of gaseous fuels (NG, H_2) and is subsequently embedded into a two-zone knocking model proposed in previous work [22], which enables the prediction of the engine performance and the knocking resistance during the gaseous fuel interchangeability.

In the extended zero-dimensional model, the Vibe model is used to calculate the combustion rate, which is then employed for the determination of the mass balance and instantaneous composition fraction. The properties library is built on the assumption that the thermodynamic properties of the in-cylinder gas are functions of the composition and the temperature, which provides the combustion heat, the internal energy, the enthalpy and the specific heat. The heat release rate is obtained by multiplying the combustion heat with fuel burning rate. The heat transfer coefficient in Heat Loss sub-model is estimated by using the Woschni formula. The in-cylinder temperature is calculated by employing the First Law of Thermodynamics.

The overall model consists of a two-zone module for representing the combustion phase and a single-zone module for modelling the compression and expansion phases. Both modules are developed based on the extended single-zone zero-dimensional model. The combustion submodel uses the multi-Vibe function to estimate the heat release rate. The in-cylinder parameters, including the air fraction, as well as the pressure and temperature of the unburnt zone are used to as input to calculate the knocking parameters.

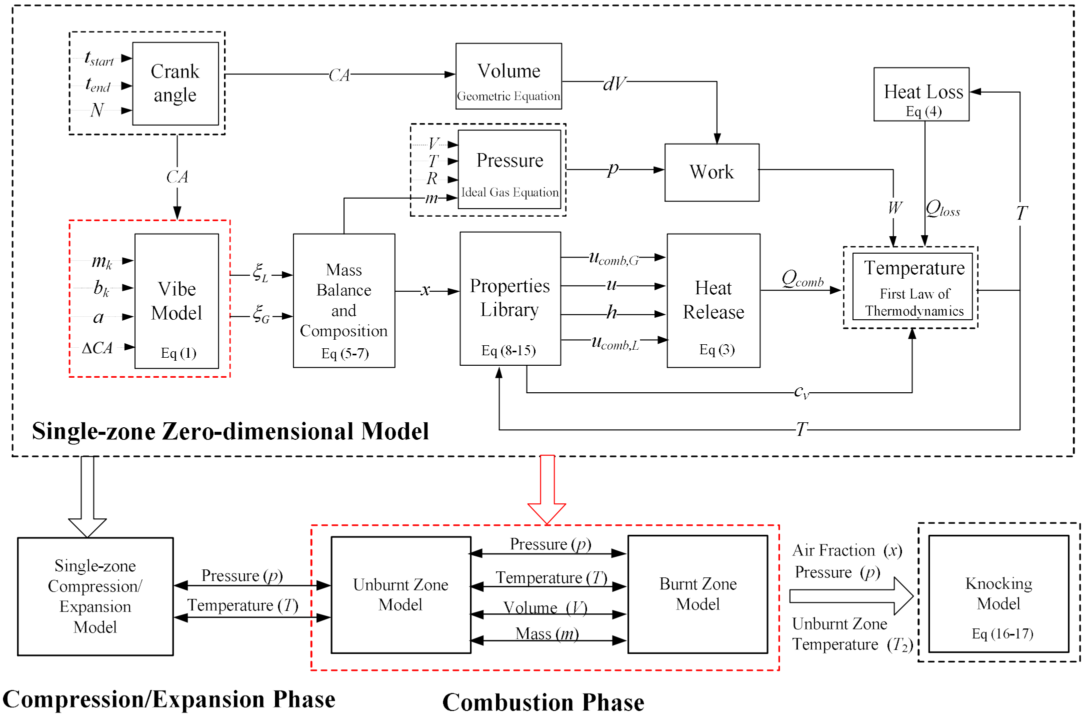

Figure 1. Calculation flowchart of the prediction model for gaseous fuels interchangeability

2.3 Model Setup

The geometric dimensions are the primary input of the proposed single-zone model. The engine rotational speed and the injected fuel mass need to be provided for determining the working conditions of the investigated internal combustion engines. The in-cylinder pressure and temperature at IVC are used to calculate the gas mass trapped in the cylinder at IVC. The charge efficiency is defined as the mass ratio of the fresh air and the total trapped gas, which considers the existence of residual gas from previous working cycle. The employed fuels (liquid or gaseous) along with their compositions needs to be provided as input. For the combustion simulation of a direct-injection liquid fuel engine, the injection pressure is essential to evaluate the specific energy (e_f) caused by the injection pressure difference and the evaporation. In addition, the wall temperatures of the cylinder head, the cylinder liner and the piston top need to be set. In the *Combustion Model*, the Vibe parameters are required to calculate the heat release rate. The simulation period is set from the IVC to the exhaust valve opening (EVO), whilst the simulation step is set to be 0.5°CA. The crank angle is obtained from the time integration of the rotational speed assuming that the rotational speed remains constant. In addition, the fourth-order Runge-Kutta algorithm is used as the equations solver. Table 1 shows the input parameters of the single-zone model.

Table 1. Single-zone model input parameters

Geometric dimensions	Bore [m]	Fuel parameters	Composition
	Stroke [m]		Injection pressure [bar]
	Compression ratio [-]		
	Connecting rod length [m]	Combustion model	*SOC, EOC* [°CA]
	IVC timing [°CA]		b_i
	EVO timing [°CA]		$m_{v,i}$
Working condition	Rotational speed [r/min]	Heat loss model	T_{head} [K]
	Injected fuel mass [kg/cycle/cylinder]		T_{liner} [K]
			T_{piston} [K]
Initial conditions	Pressure [bar]	Simulation parameters	Duration
	Temperature [K]		Step
	Charge efficiency [-]		Solver

For the two-zone knocking prediction model, three more parameters (S_{mass}, λ_{ent} and S_{HH}) need to be provided as input besides the parameters shown in Table 1. The initial mass coefficient S_{mass} is defined as the ratio of the initial mass of the burnt zone and the overall cylinder zone, whereas λ_{ent} and S_{HH} are used to describe the mass and energy flow between the two gas phase zones. The entrainment factor λ_{ent} is introduced to account for the existence of the stoichiometric gas in the unburnt zone and the possibility that the excess air ratio entrained from the unburnt zone to the burnt zone could be more than or less than

1. The Heider–Holhbaum factor S_{HH} [22] is defined as the ratio of the stoichiometric gas flow leaving the burnt zone and the stoichiometric gas production rate.

2.4 Combustion Model Calibration

As the combustion characteristics varies with the engine working conditions, the combustion model needs to be calibrated before being used to predict the engine performance. In this study, heat release analysis is applied to determine the Vibe parameters, which are then used to simulate the fuel burning rate of single-fuel engines or multi-fuel engines.

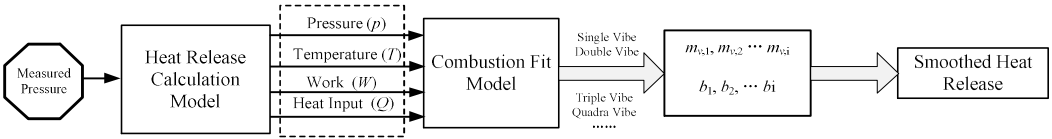

Figure 2. Calculation flowchart of the combustion model calibration[23]

Sui [23] proposed a way to calculate the heat release rate of diesel engines by applying an inverse in-cylinder model. Figure 2 presents the calculation flow of the combustion model calibration, which can be illustrated as follow.

1) The heat release rate can be obtained from the HRR analysis by using the measured in-cylinder pressure by employing heat release calculation model. Alternatively, Computational Fluid Dynamics (CFD) simulation tools can be used to estimate the heat release rate in case the measured pressure is not available.
2) For representing the obtained heat release rate with the combustion fit model, the number of the adopted Vibe functions needs to be determined according to the involved fuel types and the fuel injection method. In order to reduce the parameters number, the combustion start timing for all the gaseous fuels are considered to be the same. Then a curve fit method is applied to identify the Vibe parameters, including the start of combustion (*SOC*), the end of combustion (*EOC*), weight factors (b_i) and shape factors ($m_{v,i}$). a is set at 6.9078 to maintain a combustion efficiency of 99.9%.
3) The HRR obtained by employing the approach described above provides a smoother HRR than the one calculated from the in-cylinder pressure by using filtering. Thus, it is more suitable for the in-cylinder combustion modelling as the measurement fluctuations are eliminated [23].

3. Model Validation

As a number of issues may occur during the operation of gaseous fuel engines, such as the deteriorated engine dynamic behaviour as well as knocking or misfiring tendency, the fuel flexibility is proposed as a counter measure in gas or dual-fuel internal combustion engines like diesel-natural gas engines [38] and diesel-H_2-natural gas engines [39] As the proposed model is based on the calculation of the working medium thermodynamic properties and multi-Vibe combustion functions, it is practically capable of predicting the performance of all types of internal combustion engines with the developed properties library and the appropriate combustion model calibration. The model validation was carried out for four internal combustion engine cases, in specific, the MAN 20/27 diesel engine, the 2135 spark-ignited natural gas engine, the YC6K dual-fuel engine and the Lister Petter TR2 diesel-H_2-natural gas engine. The experimental data of the first three engines was obtained from engine tests [27], whilst that of the Lister Petter TR2 diesel-H_2-natural gas engine was taken from [41].

3.1 Diesel Engine

In this section, the model application to diesel engines is verified by comparing the derived results against experimental data from a MAN 20/27 diesel engine. The main characteristics of the MAN 20/27 engine are shown in Table 2. ABDC represents after Bottom Dead Centre. BBDC represents before Bottom Dead Centre.

Table 2. Main characteristics of MAN 20/27 diesel engine [27]

Parameter	
Bore [mm]	200
Stroke [mm]	270
Nominal Engine Speed [rpm]	1000
Nominal power per cylinder [kW]	84
Compression Ratio	13.4:1
IVC [°CA, ABDC]	20
EVO [°CA, BBDC]	60

Figure 3(a) shows the comparison of the experimentally obtained data and the simulation results for the in-cylinder pressure of the MAN 20/27 diesel engine. As shown in Figure 3(a), the derived in-cylinder pressure sufficiently coincides with the measured one. In Figure 3(b), u_{comb} and $u_{comb,\ eff}$ represent the combustion heat calculated by Eq (13) and Eq (15), respectively. The relative error between the u_{comb} and the LHV ranges from 1.31% to 2.81%, which implies that using the LHV in simulation tools would not provide a considerable error in the calculation of the heat release and engine power. With considering the influence of the liquid fuel evaporation, $u_{comb,\mathrm{eff}}$ exhibits a sharp decrease of approximately 2.7 10^6 J/kg and a subsequent increase of 0.7 10^6 J/kg, resulting in the largest relative deviation (from the LHV) of 8.03% at around 208°CA.

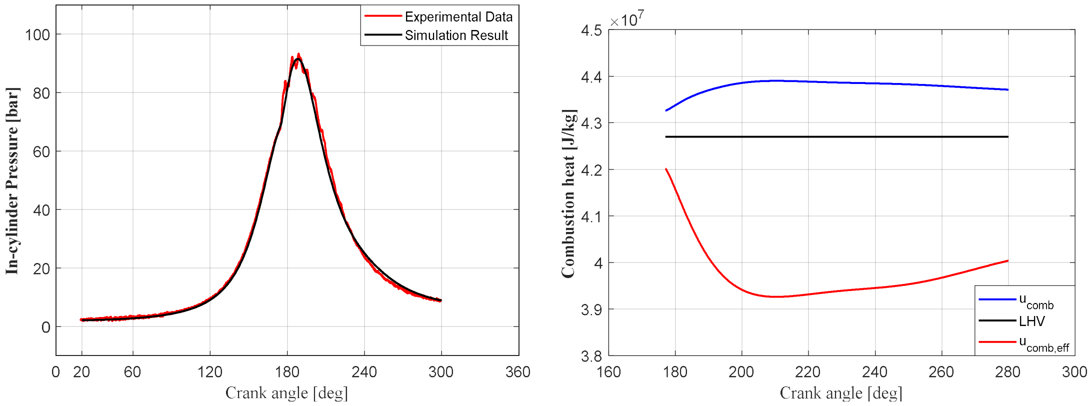

(a) (b)

Figure 3. Simulation results and comparison with available experimental data for the MAN 20/27 diesel engine operating at its nominal power and speed; (a) the in-cylinder pressure; (b) the combustion heat.

3.2 Natural Gas Engine

Experimental data from the 2135 natural gas (NG) engine is used to verify the application of the proposed method on premixed SI engines operating with natural gas. The natural gas composition and the main characteristics of 2135 engine are provided in Table 3 and

Table 4.

Table 3. Natural gas composition

Composition	Fraction (%)
CH_4	76.66
C_2H_6	17.76
C_3H_8	4.61
n-C_4H_{10}	0.41
i-C_4H_{10}	0.19

C_5H_{12}	0.06
N_2	0.31

Table 4. Main characteristics of 2135 natural gas engine

Parameter	
Bore [mm]	135
Stroke [mm]	140
Nominal Engine Speed [rpm]	1500
Nominal power per cylinder [kW]	11.92
Compression Ratio	11:1
IVC [°CA, ABDC]	48
EVO [°CA, BBDC]	48

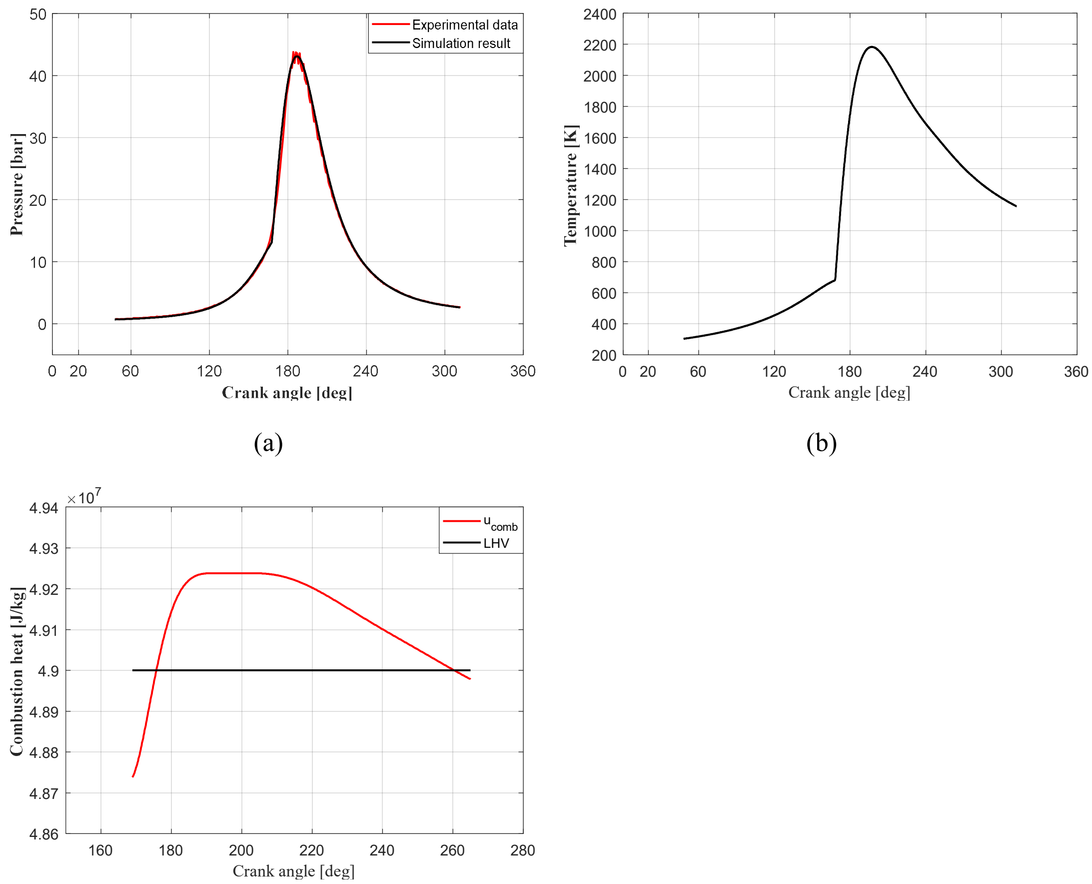

(c)

Figure 4. Simulation results and comparison with available experimental data for the 2135 natural

gas engine operating at its nominal power and speed; (a) the in-cylinder pressure; (b) the in-cylinder temperature; (c) the combustion heat.

As it can be inferred from Figure 4(a), the simulation results adequately coincide with the measured in-cylinder pressure from the 2135 natural gas engine, which verifies the accuracy of the single-zone in-cylinder model. Figure 4(b) and Figure 4(c) present the in-cylinder temperature and the combustion heat. The combustion heat varies in a same trend with the in-cylinder temperature during the combustion period as it is highly dependent on the temperature variation. In addition, u_{comb} is smaller than the LHV during the periods of 169°CA to 177°CA and 252°CA to 265°CA due to the relatively lower temperature of the in-cylinder working medium. The difference between the u_{comb} and the LHV of natural gas is quite small (less than 0.55%) comparing to that of diesel fuel in Figure 3(b), which indicates that even a constant LHV would not considerably affect the calculation accuracy.

3.3 Dual-fuel Engine

The YC6K dual fuel engine was converted from YC6K diesel engine by adding a natural gas supply system and updating its Electronic Control Unit (ECU). It works in two different modes, the diesel mode and dual-fuel mode. Diesel fuel with lower auto-ignition temperature serves as an ignition source for the natural gas combustion. The diesel fuel contributes to 25.7% of the total energy release in dual-fuel mode at the nominal working condition. The main characteristics of the YC6K dual-fuel engine are shown in Table 5. Three Vibe functions are used to simulate the heat release corresponding to the diesel fuel premixed combustion, the diesel fuel diffusion combustion and the natural gas combustion.

Table 5. Main characteristics of YC6K dual-fuel engine

Parameter	
Bore [mm]	129
Stroke [mm]	155
Nominal Engine Speed [rpm]	1800
Nominal power per cylinder [kW]	65
Compression Ratio	16.5:1
IVC [°CA, ABDC]	2

EVO [°CA, BBDC]	31

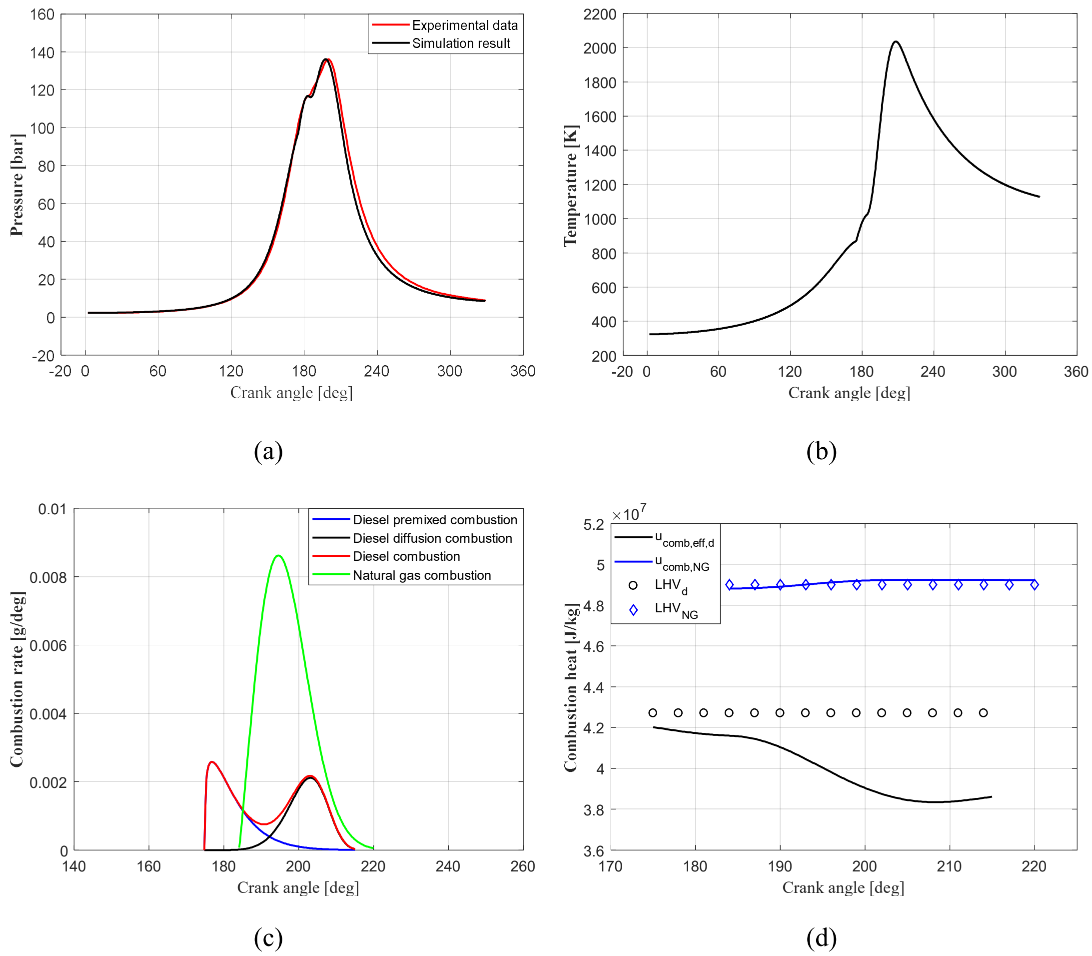

Figure 5. Simulation results and comparison with available experimental data for the YC6K dual fuel engine operating at its nominal power and speed; (a) in-cylinder pressure; (b) in-cylinder temperature; (c) combustion rates of diesel fuel and natural gas; (d) combustion heat of diesel fuel and natural gas.

Figure 5(a) presents the comparison of the derived in-cylinder pressure variation and the corresponding measured data. The measured pressure was obtained from an AVL combustion analyser, which smoothed the original pressure signal with its inbuilt algorithm. The simulation results are in sufficient coincidence with the measured pressure, whereas the predicted peak pressure crank angle is about 2.5°CA advanced in comparison with the experimental data. In this case, the dominant combustion phase is retarded after the top dead centre by delaying the diesel injection timing in order to decrease the average in-cylinder temperature for reducing the NO_x emissions. As can be inferred from Figure 5(b), the in-cylinder temperature is roughly controlled under 2000 K, which is the threshold that the thermal NO_x

begins to form rapidly [42].

Figure 5(c) shows the estimated total heat release rate, which consists of three parts corresponding to the diesel fuel premixed combustion, the diesel fuel diffusion combustion and the natural gas premixed combustion, respectively. One single Vibe function is used to characterize the combustion rate of natural gas as it exhibits a premixed combustion behaviour [43]. In order to reduce the employed Vibe function parameters number, the start and end timings of premixed combustion and diffusion combustion of the diesel fuel are assumed to be the same. The start timing of the natural gas combustion is set at 8°CA after that of the diesel fuel. Figure 5(d) shows the effective combustion heat variations of the diesel and the natural gas fuels. The considerable drop (during 175°CA ~207°CA) caused by the liquid diesel fuel evaporation can be easily spotted on the combustion heat of diesel fuel. By multiplying the combustion heat by combustion rate, it can be inferred that the diesel fuel contributes 25.7% of the total energy release.

3.4 Tri-fuel Engine

Lean burn technology is now widely used in NG engines to decrease the average in-cylinder temperature for reducing the NOx emissions. However, due to the slow flame speed of the NG mixture, operational limitations of the engine settings (air-fuel ratio, injection/spark timing, etc.) must be imposed for to ensure the smooth engine operation and low controlled emissions. In this respect, meeting the existing and future emissions regulations without compromising the engine efficiency is a quite challenging task [44], which depends on the engine type and application [45]. The enrichment of NG with a fast-burning fuel, i.e. hydrogen, which has a laminar burning velocity sevenfold higher than that of the NG and a low ignition energy limit, was reported to be an effective method to extend the lean operation limit of the NG engines [41].

Abu-Jrai [41] carried out an experimental study by using a Lister Petter TR2 engine to study the effect of tri-fuel (Ultra Low Sulfur Diesel (ULSD), H_2 and CH_4) operation on the combustion characteristics. Engine tests using 20% (volumetric percentage of the total air inlet charge) H_2-CH_4 mixture injected in the inlet ports and direct injected ULSD were performed in three engine loads (25%, 50% and 75%) at a constant engine speed of 1500 rpm. The total air-fuel equivalence ratio was controlled and was set at 1.4 for all the testing conditions. Part of the experimental data in [41] is used in this study to verify the model applicability to the tri-fuel engines. The selected experimental data was measured at

1500 rpm and 75% load when the Lister Petter TR2 tri-fuel engine operated on two gaseous fuel-air mixtures (H50M50 and H75M25, respectively) and the ULSD. The constituents of H50M50 are 10% H_2, 10% CH_4 and 80% air, whilst the H75M25 consists of 15% H_2, 5% CH_4 and 80% air. Table 6 shows the main characteristics of the Lister Petter TR2 tri-fuel engine.

Table 6. Main characteristics of Lister Petter TR2 engine[41]

Parameter	
Bore [mm]	98.42
Stroke [mm]	101.6
Nominal Engine Speed [rpm]	1500
Nominal power per cylinder [kW]	6.05
Compression Ratio	15.5:1
IVC [°CA, ABDC]	32
EVO [°CA, BBDC]	76

Four Vibe functions are employed to calculate the HRR of the tri-fuel engine. This approach requires 16 Vibe parameters to be determined as listed in Table 7. In order to reduce the Vibe parameters number, the weight factors estimated for the 20/27 diesel engine combustion (b_1 and b_2) are used to represent the premixed combustion stage and diffusion combustion stage of the ULSD. The shape factors estimated for the 20/27diesel engine combustion (m_1 and m_2) and the 2135 NG engine combustion (m_3) are used to simulate the heat release rate of ULSD and CH_4 in the tri-fuel engine combustion model. In addition, the H_2 and CH_4 are assumed to start combustion at the same timing and have the same combustion duration. The combustion start timings of the ULSD (SOC_1 and SOC_2) and the gaseous fuels (SOC_3 and SOC_4) can be deduced from the sharp increasing points on the measured HRR curves. The remaining three Vibe parameters m_4, $\Delta\theta_1$ (also equal to $\Delta\theta_2$) and $\Delta\theta_3$ (also equal to $\Delta\theta_4$) are obtained by employing a curve fitting method. It is inferred from Table 7 that the gaseous fuels with higher H_2 content start combustion 1°CA earlier, which is accompanied with shorter combustion durations for the diesel, CH_4 and H_2 fuels.

Table 7. Vibe parameters for HRR calculation in the tri-fuel engine model

	SOC_1	SOC_2	SOC_3	SOC_4	$\Delta\theta_1$	$\Delta\theta_2$	$\Delta\theta_3$	$\Delta\theta_4$
H50M50	176.5	176.5	180.5	180.5	22	22	10	10

H75M25	176.5	176.5	179.5	179.5	10	10	7.5	7.5
	m_1	m_2	m_3	m_4	b_1	b_2		
H50M50	0.4	3	1.5	1.0	0.88	0.12		
H75M25	0.4	3	1.5	1.0	0.88	0.12		

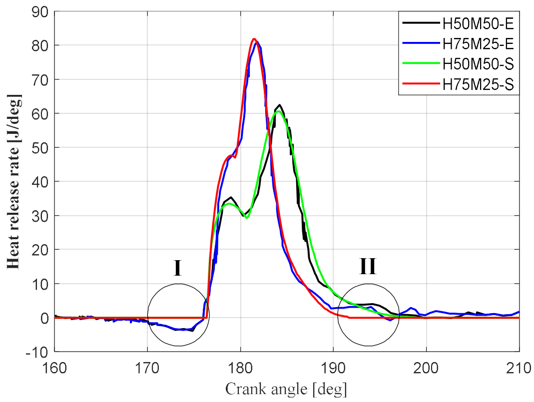

(a)

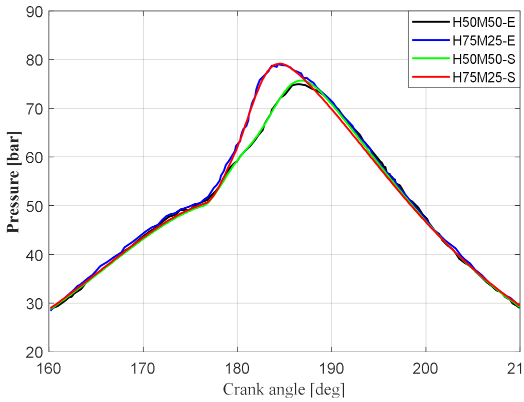

(b)

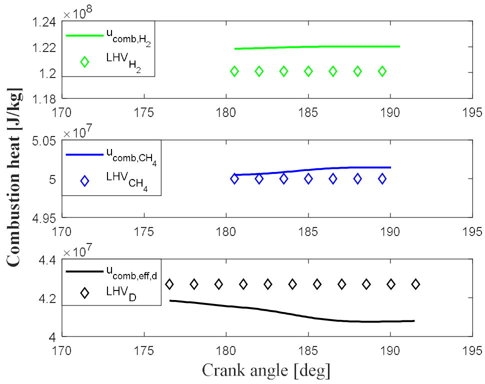

(c)

Figure 6. Simulation results and comparison with available experimental data for the Lister Petter TR2 tri-fuel engine operating at 1500 rpm and 75% load with H50M50 and H75M25 mixtures; (a) heat release rate; (b) in-cylinder pressure; (c) combustion heat.

Figure 6 shows the comparison of the simulation results with the respective experimental data for the tri-fuel engine with H50M50 and H75M25 fuel mixtures. In this figure, **E** represents the experimental data from literature [41], whilst **S** denotes the simulation results. The Vibe parameters in Table 7 were used to simulate the heat release rate of the tri-fuel engine, which adequately matches the experimental data during the dominant combustion phase except the zone I and Zone II parts, as shown in Figure 6(a). The deviation between the simulation and experimental data in Zone I is mainly attributed to the liquid diesel fuel evaporation, which starts earlier than the combustion start, as an injection model is not used in this study. The difference in Zone II is due to the heat loss that is included in the heat release calculated from the experimentally obtained cylinder pressure, but not being considered for the calculation of the net heat release in the developed model.

As can be deduced from Figure 6(b), the simulation results sufficiently agree with the measured in-cylinder pressure for the investigated cases. Higher H_2 percentage tends to achieve a greater peak cylinder pressure in an advanced crank angle than the respective ones in the case of a fuel mixture with a lower H_2 percentage. This is attributed to the high hydrogen burning velocity, which result in a faster and advanced heat release after the diesel fuel ignition, as shown in Figure 6 (a).

Figure 6(c) shows the combustion heat of the H_2, the CH_4 and the ULSD in comparison with their LHVs. The combustion heat of H_2 is much higher than that of other fuels due to its extremely small molar mass. The effective combustion heat of the liquid diesel fuel exhibits a decrease with a maximum relative deviation of 8.03% compared to its LHV, whilst that of H_2, CH_4 slightly increase exhibiting a maximum relative deviation of 1.67% and 0.3%, respectively compared to their LHVs.

3.5 Quantitative Comparison

Four in-cylinder parameters are chosen as criteria to verify the accuracy of the proposed single-zone zero-dimensional model quantitatively, in specific, the Indicated Mean Effective Pressure (IMEP), the pressure at EVO (p_{EO}), the peak pressure (p_{max}) and the corresponding crank angle (α_1). IMEP, p_{max} and p_{EO} are related to the mechanical load and heat load of the cylinder to a certain extend. The comparison of the simulation results and the experimental data is shown in Table 8. The error of α_1 is presented in the form of absolute difference (°CA), whilst that of p_{max} and p_{EO} are indicated by the absolute error percentage (%). In addition, p_{EO} for the tri-fuel engine case in Table 8 is actually the pressure value at 30°CA after top dead centre (ATDC), as Abu-Jrai [41] provided the in-cylinder pressure from 20°CA before top dead centre (BTDC) to 30°CA ATDC instead of the complete in-cylinder process. The IMEP comparison of the tri-fuel engine is not included in Table 8 due to the same reason. As can be seen from Table 8, the relative errors of IMEP, p_{max} and p_{EO} are below 3%, whilst the absolute difference of the peak pressure position are less than 3°CA. Thus, it can be inferred that the proposed in-cylinder single-zone model is able to predict the performance of internal combustion engines operating with flexible fuels and can be used with fidelity for the calculation presented in the next section.

Table 8. The quantitative comparison of p_{max} and p_{EO} between the simulation and the measurement

	Parameters	IMEP (bar)	p_{EO} (bar)	p_{max} (bar)	α_1 (°CA ATDC)
Diesel engine	Simulation	11.96	8.88	91.54	8.1
	Measurement	12.02	8.93	93.33	9.7
	Error [% or °CA]	0.55	0.56	1.92	1.6
Natural gas engine	Simulation	4.65	2.44	44.22	4.0
	Measurement	4.76	2.51	44.31	7.0
	Error [% or °CA]	2.35	2.79	0.20	3.0
Dual-fuel engine	Simulation	21.00	8.52	136.00	16.8
	Measurement	21.39	8.76	136.10	19.0
	Error [% or °CA]	1.84	2.74	0.07	2.2
Tri-fuel engine (H50M50)	Simulation		29.19	75.71	6.8
	Measurement		29.05	74.96	6.5
	Error [% or °CA]		0.48	1.00	0.3
Tri-fuel engine (H75M25)	Simulation		29.47	79.17	4.5
	Measurement		29.43	79.02	4.3
	Error [% or °CA]		0.14	0.19	0.2

4. Investigation on the Gaseous Fuel Interchangeability

The Wobbe Index has been widely-used in practice as an unambiguous reference to assess the interchangeability of gaseous fuels. According to the WI definition, the energy supplied to the engine remains constant when the WI holds the same values for a constant engine air flow. Nevertheless, the WI just provides a rough prediction of the involved fuel energy, which is not enough to evaluate the engine performance with sufficient accuracy. In addition, inert gases like CO_2 and N_2 are often added to the raw natural gas to maintain a constant WI in order to meet the fuel interchangeability requirements as well as for avoiding controlling the variation of engine settings (i.e. spark timing or pilot fuel injection start). The knocking resistance of a gaseous fuel-air mixture depends on its composition, the engine load, the trapped air-fuel ratio and the temperature of the unburnt zone [10]. Thus, the addition of inert gases affects the engine knocking performance as the decreased LHV could reduce the in-cylinder temperature.

In this section, the developed engine model is employed to investigate the engine performance in cases where fuels (or gaseous fuels mixtures) with the same WI are used. In addition, the inert gas addition on engine knocking performance is investigated.

4.1 Engine Performance Prediction using fuels with the same Wobbe Index

In this section, the model as presented in the previous section is used to investigate the energy input and the engine power of the 2135 engine operating on three gaseous fuels with same WI. The composition and properties of the employed gaseous fuels were taken from [10], and shown in Table 9. As the fuel composition does not noticeably influence the combustion velocity [10], the heat release rate can be considered the same for the three investigated cases. The theoretical energy input of each cylinder is fixed at 3.8 kJ as it provides an approximate power of 11.92 kW. Then, the mass flow of the gaseous fuel and air can be calculated according to the fuel LHV considering that the air-fuel ratio is kept at its stoichiometric value as presented in Table 9. LPG represents liquefied petroleum gas.

Table 9. Fuel composition and properties of the investigated gaseous fuels [10]

	Volumetric fraction (%)				Heating value		WI	Stoichiometric air-fuel ratio
	CH_4	C_3H_8	CO_2	N_2	MJ/m^3	MJ/kg	MJ/m^3	[-]
Natural gas	81	2	3	14	31.68	38.11	39.47	12.62
LPG-CO_2	-	54	46	-	50.33	23.95	39.47	8.59
LPG-N_2	-	47	-	53	43.81	27.52	39.47	9.26

Table 10 shows the comparison of the theoretical values and the simulated results for the heat release and the engine power. The simulated energy input of the LPG-CO_2 mixture is 5.53% higher than its theoretical value, whilst the ones of the natural gas and the LPG-N_2 mixture are 5.26% and 1.05% lower than their theoretical values, respectively. Despite the 1.05% decrease from the theoretical energy input, the predicted engine power when the engine operates with LPG-N_2 mixture is 2.77% higher than its reference value. The derived engine power of the NG and the LPG-CO_2 mixture are 3.02 % lower and 8.98 % higher than their theoretical values respectively, which are in accordance with the relative error trend of their heat release.

Table 10. The energy input and the engine power with three gaseous fuels

	Heat release			Engine power		
	Theoretical value (kJ)	Calculated value (kJ)	Relative error (%)	Reference value (kW)	Calculated value (kW)	Relative error (%)
NG	3.80	3.60	-5.26	11.92	11.56	-3.02
LPG-CO_2	3.80	4.01	5.53	11.92	12.99	8.98
LPG-N_2	3.80	3.76	-1.05	11.92	12.25	2.77

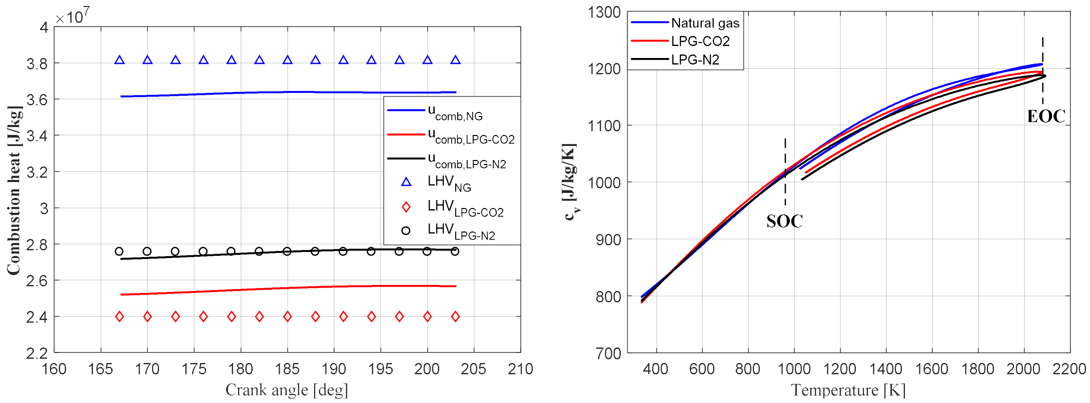

(a) (b)

Figure 7. Simulation results for the 2135 engine operating at nominal conditions with natural gas, LPG-CO_2 mixture and LPG-N_2 mixture; (a) combustion heat versus crank angle; (b) specific heat of the in-cylinder gases versus in-cylinder temperature.

Figure 7(a) presents the combustion heat variation with the crank angle for the three investigated gaseous fuels. As deduced from Figure 7(a), the combustion heat of the LPG-N_2 mixture roughly equals to its LHV, leading to the smallest relative error for the heat release and the engine power when the 2135 engine operates with LPG-N_2 mixture. The average combustion heat of the NG is about 5.3% lower than its LHV, whilst the average combustion heat of the LPG-CO_2 mixture is approximately 5.5% higher than its LHV, which matches to the engine power variation trend.

Figure 7(b) shows the specific heats at constant volume of the in-cylinder gases as functions of the in-cylinder temperature. The high content of the H_2O vapour in the NG combustion products results in a higher specific heat than that of the other mixtures during the combustion phase. With regard to the comparison between the LPG-CO_2 and the LPG-N_2 mixtures, the greater amount of CO_2 that has a higher specific heat results in a greater specific heat of the LPG-CO_2 mixture (the latter is higher in comparison with that of the LPG-N_2 mixture).

4.2 Influence of Inert Gas Addition on Knocking Performance

In this section, the influence of the CO_2 and N_2 addition on the knocking performance of the 2135 engine operating on natural gas is investigated. The Adu Dhabi natural gas [46], which has one of the lowest knock resistances because of its high ethane content, is used as the baseline gaseous fuel herein, whilst the volumetric addition of CO_2 and N_2 is set to be 5%, 10%, 15% and 20%, as shown in Table 11. Motor Octane Numbers (MON) of the fuel-inert gas mixtures are obtained according to the equation for MON and MN [46, 47]. The fuel consumption rate in each case is calculated referring to the fact that the volumetric flow of the gaseous fuel is inversely proportional to the square root of its density for a naturally aspirated premixed engine.

Table 11. Composition and MON of natural gas with different inert gas additions

Volumetric Fraction (%)	Natural gas	CO_2 addition				N_2 addition			
		+ 5%	+ 10%	+ 15%	+20%	+ 5%	+ 10%	+ 15%	20%
CH_4	82	77.9	73.8	69.7	65.6	77.9	73.8	69.7	65.6
C_2H_6	15.8	15.01	14.22	13.43	12.64	15.01	14.22	13.43	12.64
C_3H_8	2.2	2.09	1.98	1.87	1.76	2.09	1.98	1.87	1.76
CO_2	0	5	10	15	20	0	0	0	0
N_2	0	0	0	0	0	5	5	15	20
MON	119.2	122.4	125.7	128.9	132.2	120.3	121.4	122.5	123.6

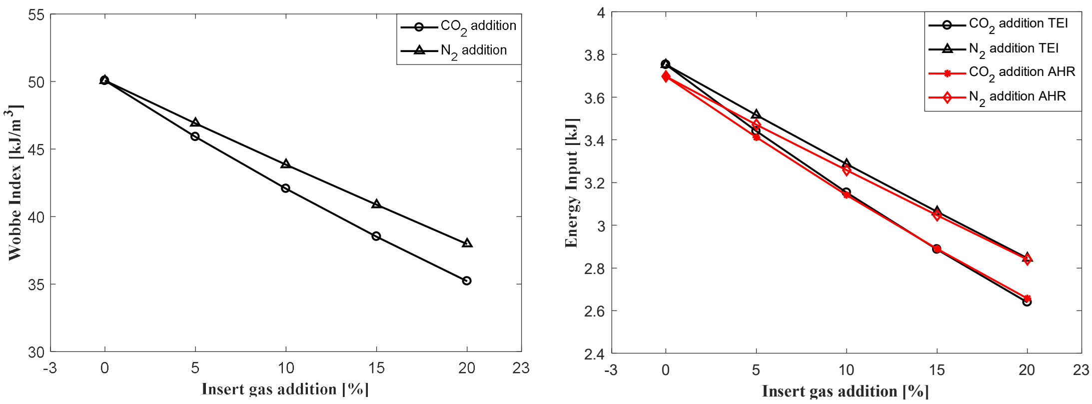

(a) (b)

Figure 8. Simulation results for the 2135 engine operating on natural gas with 5%, 10%, 15% and 20% addition of CO_2 and N_2; (a) Wobbe Index variation; (b) Energy input variation.

Figure 8(a) shows the Wobbe Index variation of the natural gas with 0%, 5%, 10%, 15% and 20% CO_2 and N_2 additions, respectively. As shown in Figure 8(a), in both cases the Wobbe Index decreases almost linearly with the increase of the CO_2 and N_2 addition. CO_2 proves to be more effective than N_2 in the Wobbe Index reduction as the CO_2 density is about 1.6 times the N_2 density under standard conditions (p=101.325 kPa, T=273.15 K).

In Figure 8(b), the derived (for an engine cylinder) Theoretical Energy Input (TEI) and the Accumulated Heat Release (AHR) variations with different inert gas addition volumetric percentages are presented. The TEI is calculated by the LHV and the supplied fuel mass, whilst the AHR is obtained from the simulation model. As the input of the chemical fuel energy is directly proportional to the value of the Wobbe Index for a naturally aspirated premixed engine, both TEI values with the CO_2 and N_2 additions appear to decease in the same trend with the WI variation shown in Figure 8(a). In addition, the AHR values for all cases are smaller than the corresponding TEI values (except for the case of 20%(vol) CO_2 addition), as they are calculated by the internal energy difference of the combustion reactants and products as function of the average in-cylinder gas temperature, which is much greater than the temperature in standard conditions.

As the detection of knocking onset in NG engines might be sensitive to the simulation step, various simulation step values (0.5°CA, 0.2°CA and 0.1°CA) were tested to investigate the effects of the simulation step on the knocking onset. However, the knocking onset remains at 15°CA ATDC, which indicates that the investigated simulation step values did not affect considerably the knocking onset. This is attributed to the fact that the knocking prediction is based on an empirical knocking formula and a two-zone model, which is relatively simplified and does not rely much on the simulation step. Thus, the following simulation works for the knocking prediction are performed with a fixed simulation step of 0.5 °CA.

Figure 9(a) shows the natural induction time integral with varying inert CO_2 and N_2 addition rates, which indicates the occurrence of knocking phenomenon when it reaches unity. As shown in Figure 9(a), the addition of CO_2 causes a significant decrease of the final value of the natural induction time integral, whilst the N_2 addition results in a relatively smaller decrease of the natural induction time. Figure 9(b) shows the knocking index, which provides the relative knocking probability with different inert gases addition rates. The knocking index with 0% inert gas addition is set to 100 as it represents the baseline condition. It can be inferred from Figure 9(b) that both the CO_2 addition and the N_2 addition can reduce the knocking probability of the natural gas engine with different levels. The CO_2 addition seems to be more effective than N_2 in eliminating the knocking phenomenon, as the knocking index decreases to zero with a 16% CO_2 addition, whilst the knocking index with 20% N_2 addition remains at 17.

Figure 9(c) and Figure 9(d) show the knocking position and knocking intensity with different inert gases (CO_2 and N_2) addition rates. These two parameters are presented in the form of the crank angle after the cylinder top dead centre (ATDC) and the mass fraction of the unburnt fuel in unburnt zone when the knocking phenomenon happens, respectively. The knocking position is retarded by 19°CA with 15%(vol) CO_2 addition. For a CO_2 addition over 16% (vol), knocking does not occur, therefore, knocking position is not shown in Figure 9 (c). The knocking intensity decreases from 21.5% to 0% when the CO_2 addition increases from 0% to 16%. The N_2 addition from 5% to 20% retards the knocking position by 10.5°CA and decreases the knocking intensity by 12%.

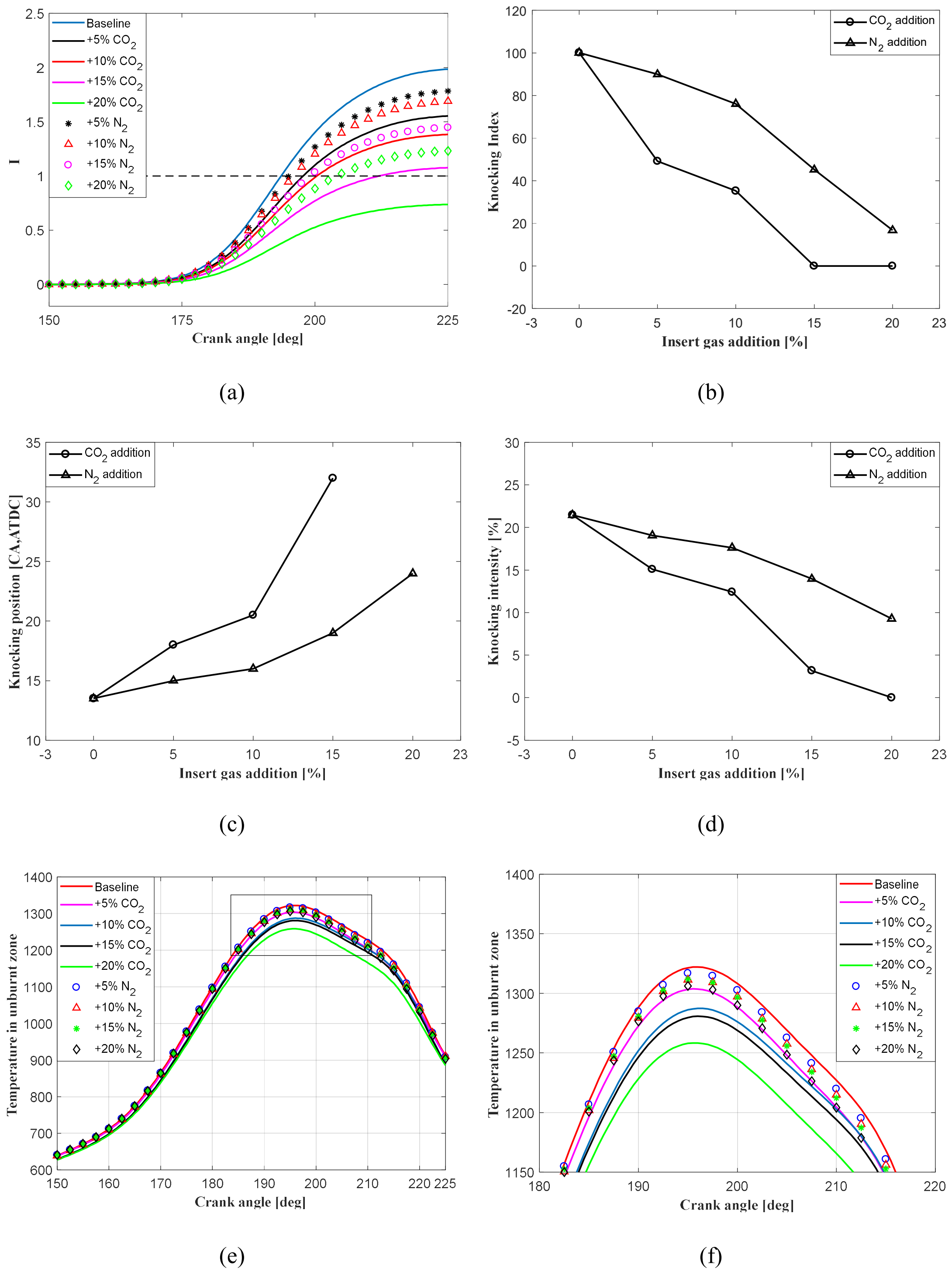

Figure 9. Simulation results for the 2135 engine operating on natural gas with 5%, 10%, 15% and 20% addition of CO_2 and N_2; (a) natural induction time integration; (b) knocking index; (c) knocking position; (d) knocking intensity; (e) the average temperature in unburnt zone (original); (f) the average temperature in unburnt zone (zoom in).

Figure 9(e) and Figure 9(f) present the gas temperatures of the unburnt zone with different inert gas addition rates. The unburnt zone gas temperature reduces with the increase of the CO_2 and N_2 addition rates, which results in the knocking probability reduction according to Eq (17). As CO_2 has higher specific heat capacity and higher density than the N_2 ($\rho_{CO_2} = 1.977$ kg/m^3, $\rho_{N_2} = 1.25$ kg/m^3 at standard conditions), the CO_2 addition more significantly reduces the unburnt zone temperature, resulting in better knocking resistance.

5. Conclusions

This study proposed an extended zero-dimensional model capable of simulating the multi-fuel internal combustion engines, which employs the calculation of the thermodynamic properties of multiple fuel mixtures and their combustion products. Subsequently, the extended model was used to investigate the interchangeability between gaseous fuels with same WI and the influence of the inert gases (CO_2 and N_2) addition on the engine knocking resistance. The main findings of this study are summarised as follow.

1. The maximum error between the simulation results and the respective experimental data was in the range of 3% (obtained for the prediction of the in-cylinder pressure) implying that the extended model shows adequate accuracy in predicting the operating parameters of the investigated internal combustion engines operating on single or multiple fuels, including diesel engines, natural gas spark-ignited engines, dual fuel engines and tri-fuel engines.
2. In terms of the energy input and the engine power, the relative errors between the WI estimation and the results obtained by the developed model can be as high as 5.53% and 8.98% respectively, which implies that simulation tools of adequate accuracy must be used for the engine performance prediction with fuels interchangeability to avoid possible errors occurring by considering the WI.
3. The knocking probability of the 2135 NG engine is eliminated when the CO_2 addition rate increases to around 16%, which is accompanied with a delay of 19°CA for the knocking crank angle and a decrease of 21.5% for the knocking intensity.
4. The N_2 addition from 5% to 20%, it retards the knocking position by 10.5°CA and decreases the knocking intensity by 12%.
5. Based on the preceding points, it is concluded that the CO_2 addition is more effective than the N_2 addition for suppressing the engine knocking in the investigated natural gas engine.

The proposed model extension in this paper is based on thermodynamic properties estimation and multi-Vibe functions, which are practically applicable to the zero-dimensional model development of all types of internal combustion engines, especially for those operating with flexible fuels. Compared to the traditional WI method, it provides more accurate and detailed information of the fuel interchangeability influence on engine performance and knocking resistance and therefore it is expected that the proposed model will be a useful tool that can be used in the analysis of multi-fuel engines.

Acknowledgements

This project partly is financially supported by 'International Science & Technology Cooperation Program of China', 2014DFG72360; National Key R&D Program of China, 2016YFC0205203. The second author greatly acknowledges the financial support by the MSRC sponsors DNV GL and RCCL.

Abbreviations

ABDC	After Bottom Dead Centre
AGA	American Gas Association
AHR	Accumulated Heat Release
ATDC	After Top Dead Centre
BBDC	Before Bottom Dead Centre
BTDC	Before Top Dead Centre
CA	Crank Angle
CFD	Computational Fluid Dynamics
DFT	Density Functional Theory
ECU	Electronic Control Unit
EVO	Exhaust Valve Open
EOC	End of Combustion
HRR	Heat Release Rate
HV	Heating Value
IMEP	Indicated Mean Effective Pressure
IVC	Intake Valve Close
LHV	Lower Heating Value
LPG	Liquefied Petroleum Gas
MN	Methane Number
MON	Motor Octane Number
NG	Natural Gas
ON	Octane Number
PM	Particulate Matter
SI	Spark-Ignited
SOC	Start of Combustion

TDC	Top Dead Centre
TEI	Theoretical Energy Input
THC	Total Hydrocarbons
ULSD	Ultra Low Sulphur Diesel
WI	Wobbe Index

Symbols

$A_{wall,i}$	the heat transfer surface area, [m^2]
Q_{comb}	the total heat release, [J]
Q_{loss}	the total heat loss, [J]
T	the average in-cylinder temperature, [K]
T_{norm}	the reference temperature for the thermodynamic property fitting equations, [K]
T_{shift}	the shift temperature for the thermodynamic property fitting equations, [K]
T_2	the average temperature of the unburnt zone, [K]
$T_{wall,i}$	the average wall temperature, [K]
a	the coefficient related to the combustion efficiency in Vibe function, [-]
a_k	the fitting coefficient for the specific heat at constant pressure, [-]
$\alpha_{g\rightarrow w}$	the instantaneous heat transfer coefficient from the in-cylinder gas to the walls, [J/K/m^2]
b_i	the weigh factor of each fuel, [-]
c_p	the specific heat at constant pressure, [J/kg/K]
c_v	the specific heat at constant volume, [J/kg/K]
e_f	the specific energy variation caused by the liquid fuel injection and evaporation, [J/kg]
f_c	the property parameter (c_v, h and u) for each basic species, [-]
h	the specific enthalpy, [J/kg]
$h_{f,liquid}^{in+}$	the specific enthalpy of the liquid fuel, [J/kg]
h_j^{ref}	the specific enthalpy at standard condition, [J/kg]
$\dot{m}_{f,in}$	the diesel flow rate, [kg/s]
m_0	the mass of the in-cylinder gas mixture at IVC, [kg]
m_i	the injected fuel mass of each fuel, [kg]
m_v	the shape factor in Vibe function, [-]
p	the average in-cylinder pressure, [pa]
t	the elapsed time from the start of the compression process in unburnt zone, [s]
t_{i}	the time of auto-ignition timing, [s]
τ	the natural induction time, [ms]
τ_v	the normalized combustion time, [-]
u	the specific energy, [J/kg]
u_a	the specific internal energy of air, [J/kg]
u_{comb}	the combustion heat, [J/kg]

$u_{comb,G}$	the combustion heat of the gaseous fuel, [J/kg]
$u_{comb,L}$	the combustion heat of the liquid fuel, [J/kg]
$u_{comb,eff}$	the effective combustion heat, [J/kg]
u_f	the specific internal energy of fuel, [J/kg]
u_j^{ref}	the specific internal energy at standard condition, [J/kg]
u_{sg}	the specific internal energy of stoichiometric gas, [J/kg]
x_a	the air mass fraction, [%]
x_b	the burnt fuel fraction, [%]
x_f	the fuel mass fraction, [%]
x_{sg}	the mass fraction of the combustion products, [%]
x_c	the mass fraction of the considered mixtures constituents, [%]
x_e	the mass fraction of air, gaseous fuel and stoichiometric gas, [%]
x_0	the air mass fraction at IVC, [%]
x_1	the mass fraction of the air-fuel mixture at IVC in premixed engines, [%]
σ	the stoichiometric ratio, [-]
ξ	the fuel burning rate, [kg/s]
ξ_G	the fuel burning rate of the gaseous fuel, [kg/s]
ξ_L	the fuel burning rate of the liquid fuel, [kg/s]
θ	the normalized temperature, [-]
θ_{ref}	the normalized reference temperature, [-]

References

1. Mavrelos, C. and G. Theotokatos, *Numerical investigation of a premixed combustion large marine two-stroke dual fuel engine for optimising engine settings via parametric runs.* Energy Conversion and Management, 2018. **160**: p. 48-59.
2. Barati, M.R., et al., *Comprehensive exergy analysis of a gas engine-equipped anaerobic digestion plant producing electricity and biofertilizer from organic fraction of municipal solid waste.* Energy Conversion and Management, 2017. **151**: p. 753-763.
3. Thomson, H., J.J. Corbett, and J.J. Winebrake, *Natural gas as a marine fuel.* Energy Policy, 2015. **87**: p. 153-167.
4. Ghaderi, M., et al., *Design, fabrication and characterization of infrared LVOFs for measuring gas composition.* Journal of Micromechanics and Microengineering, 2014. **24**(8): p. 084001.
5. Kakaee, A.-H., A. Paykani, and M. Ghajar, *The influence of fuel composition on the combustion and emission characteristics of natural gas fueled engines.* Renewable and Sustainable Energy Reviews, 2014. **38**: p. 64-78.
6. Jahanian, O. and S. Jazayeri, *A comprehensive numerical study on effects of natural gas composition on the operation of an HCCI engine.* Oil & Gas Science and Technology–Revue d'IFP Energies nouvelles, 2012. **67**(3): p. 503-515.
7. Ortíz, J., *Fundamentos de la intercambiabilidad del Gas Natural.* Ciencia, 2014: p. 6-15.
8. Halchuk-Harrington, R. and R. Wilson, *AGA Bulletin #36 and Weaver Interchangeability Methods: Yesterday's Research and Today's Challenges*, in *Operating Section Proceeding - Gas Association*. 2006, American Gas Association: Paramus, N.J. p. 802-823.
9. Eichmann, S.C., et al., *Determination of gas composition in a biogas plant using a Raman-based sensor system.* Measurement Science and Technology, 2014. **25**(7): p. 075503.
10. Klimstra, J., *Interchangeability of Gaseous Fuels—the Importance of the WOBBE-INDEX.*

1986, SAE Technical Paper.
11. Karavalakis, G., et al., *The effect of natural gas composition on the regulated emissions, gaseous toxic pollutants, and ultrafine particle number emissions from a refuse hauler vehicle.* Energy, 2013. **50**: p. 280-291.
12. Cardona, C.A. and A.A. Amell, *Laminar burning velocity and interchangeability analysis of biogas/C3H8/H2 with normal and oxygen-enriched air.* International Journal of Hydrogen Energy, 2013. **38**(19): p. 7994-8001.
13. Honus, S., S. Kumagai, and T. Yoshioka, *Replacing conventional fuels in USA, Europe, and UK with plastic pyrolysis gases–Part I: Experiments and graphical interchangeability methods.* Energy Conversion and Management, 2016. **126**: p. 1118-1127.
14. Honus, S., S. Kumagai, and T. Yoshioka, *Replacing conventional fuels in USA, Europe, and UK with plastic pyrolysis gases–Part II: Multi-index interchangeability methods.* Energy Conversion and Management, 2016. **126**: p. 1128-1145.
15. Baldi, F., G. Theotokatos, and K. Andersson, *Development of a combined mean value–zero dimensional model and application for a large marine four-stroke Diesel engine simulation.* Applied Energy, 2015. **154**: p. 402-415.
16. Ding, Y., D. Stapersma, and H. Grimmelius, *Using parametrized finite combustion stage models to characterize combustion in diesel engines.* Energy & Fuels, 2012. **26**(12): p. 7099-7106.
17. Maurya, R.K. and P. Mishra, *Parametric investigation on combustion and emissions characteristics of a dual fuel (natural gas port injection and diesel pilot injection) engine using 0-D SRM and 3D CFD approach.* Fuel, 2017. **210**: p. 900-913.
18. Demir, U., et al., *Evaluation of zero dimensional codes in simulating IC engines using primary reference fuel.* Applied Thermal Engineering, 2015. **76**: p. 18-24.
19. Xu, S., et al., *A phenomenological combustion analysis of a dual-fuel natural-gas diesel engine.* Proceedings of the Institution of Mechanical Engineers, Part D: Journal of Automobile Engineering, 2017. **231**(1): p. 66-83.
20. Kaprielian, L., et al., *Multi-zone quasi-dimensional combustion models for Spark-Ignition engines*. 2013, SAE Technical Paper.
21. Zhen, X., et al., *The engine knock analysis–an overview.* Applied Energy, 2012. **92**: p. 628-636.
22. Xiang, L., E. Song, and Y. Ding, *A Two-Zone Combustion Model for Knocking Prediction of Marine Natural Gas SI Engines.* Energies, 2018. **11**(3): p. 561.
23. Sui, C., et al., *Mean value modelling of diesel engine combustion based on parameterized finite stage cylinder process.* Ocean Engineering, 2017. **136**: p. 218-232.
24. Bulfin, B., et al., *Thermodynamics of CeO2 thermochemical fuel production.* Energy & Fuels, 2015. **29**(2): p. 1001-1009.
25. Hutter, R., et al., *Low-Load Limit in a Diesel-Ignited Gas Engine.* Energies, 2017. **10**(10): p. 1450.
26. Ding, Y., et al., *Thermodynamics Properties Modeling of the Diesel Fuel and In-cylinder Gas for Diesel Engines to Combustion Investigation.* Energy & Fuels, 2018.
27. Ding, Y., *Characterising combustion in diesel engines*, in *TU Delft*. 2011.
28. Neto, A., et al., *Thermodynamic analysis of fuels in gas phase: ethanol, gasoline and ethanol—gasoline predicted by DFT method.* Journal of molecular modeling, 2015. **21**(10): p. 267.
29. Li, W., et al., *Experimental and theoretical analysis of effects of equivalence ratio on mixture properties, combustion, thermal efficiency and exhaust emissions of a pilot-ignited NG engine at low loads.* Fuel, 2016. **171**: p. 125-135.
30. Merker, G.P., et al., *Simulating Combustion: Simulation of combustion and pollutant formation for engine-development*. Vol. 7. 2005: Springer Science & Business Media.
31. Ghojel, J.I., *Review of the development and applications of the Wiebe function: a tribute to the contribution of Ivan Wiebe to engine research.* International Journal of Engine Research, 2010. **11**(4): p. 297-312.
32. Woschni, G., *A universally applicable equation for the instantaneous heat transfer coefficient in the internal combustion engine*. 1967, SAE Technical paper.
33. Yaws, C.L., *Handbook of Thermodynamic Diagrams, Volume 3*. Vol. 4. 1986, USA: Gulf Publication Company.
34. Borman, G.L. and K.W. Ragland, *Combustion engineering*. 1998: McGraw-Hill

Science/Engineering/Math.
35. Wang, Z., et al., *Relationship between super-knock and pre-ignition.* International Journal of Engine Research, 2015. **16**(2): p. 166-180.
36. Qi, Y., et al., *Effects of thermodynamic conditions on the end gas combustion mode associated with engine knock.* Combustion and Flame, 2015. **162**(11): p. 4119-4128.
37. Livengood, J. and P. Wu. *Correlation of autoignition phenomena in internal combustion engines and rapid compression machines*. in *Symposium (international) on combustion*. 1955. Elsevier.
38. Kakaee, A.-H., P. Rahnama, and A. Paykani, *Influence of fuel composition on combustion and emissions characteristics of natural gas/diesel RCCI engine.* Journal of natural gas science and engineering, 2015. **25**: p. 58-65.
39. Mansor, M.R.A., M.M. Abbood, and T.I. Mohamad, *The influence of varying hydrogen-methane-diesel mixture ratio on the combustion characteristics and emissions of a direct injection diesel engine.* Fuel, 2017. **190**: p. 281-291.
40. !!! INVALID CITATION !!! [38, 39].
41. Abu-Jrai, A.M., H. Ala'a, and A.O. Hasan, *Combustion, performance, and selective catalytic reduction of NOx for a diesel engine operated with combined tri fuel (H2, CH4, and conventional diesel).* Energy, 2017. **119**: p. 901-910.
42. Stiesch, G., *Modeling engine spray and combustion processes*. Vol. Heat & Mass Transfer. 2013: Springer Science & Business Media.
43. Ghojel, J., *Review of the development and applications of the Wiebe function: a tribute to the contribution of Ivan Wiebe to engine research.* International Journal of Engine Research, 2010. **11**(4): p. 297-312.
44. Yan, F., L. Xu, and Y. Wang, *Application of hydrogen enriched natural gas in spark ignition IC engines: from fundamental fuel properties to engine performances and emissions.* Renewable and Sustainable Energy Reviews, 2017.
45. Valladolid, P.G., et al., *Impact of diesel pilot distribution on the ignition process of a dual fuel medium speed marine engine.* Energy Conversion and Management, 2017. **149**: p. 192-205.
46. Brecq, G., et al., *Knock prevention of CHP engines by addition of N2 and CO2 to the natural gas fuel.* Applied thermal engineering, 2003. **23**(11): p. 1359-1371.
47. Kubesh, J., S.R. King, and W.E. Liss, *Effect of gas composition on octane number of natural gas fuels.* SAE transactions, 1993. **101**: p. 1862-1862.